Acta Metall. Sin. (Engl. Lett.)
DOI 10.1007/s40195-017-0661-9

Compositional Variants of Cu-rich Precipitate in Thermally Aged Ferritic Steel

Qingdong Liu[1,2,3] · Yihua Chen[1] · Chuanwei Li[1] · Jianfeng Gu[1,2]

Received: 9 June 2017 / Revised: 15 September 2017

Abstract Atom probe tomography was utilized to investigate Cu precipitation in a high-strength low-alloy steel isothermally aged at 500 °C for 1, 4, 16, and 64 h after water-quenching from 900 °C. With prolonged aging time, the Cu-rich precipitates (CRPs) increased in size and decreased in number density, and gradually evolved from spheroidal to elliptical in morphology. The small CRPs were rich in a high amount of Fe and a certain amount of Ni and Mn at their early nucleation stage. The large CRPs with increased size due to extensive aging contained less Fe and more Cu at their later growth stage. Additionally, Ni and Mn were both readily to segregate at the CRP/matrix heterophase interfaces, and Mn was higher in content than Ni in the precipitate interior especially when the CRPs were large in size.

KEY WORDS: High-strength low-alloy steel; Thermal aging; Cu-rich precipitate; Atom probe tomography

1 Introduction

High-strength low-alloy (HSLA) steels are widely used as structural components of ship hulls, pipelines, bridges, etc., in modern industry, which are newly designed to obtain the combination of high strength, excellent ductility, and good toughness to insure the reliability in the increasingly harsh conditions during service. Cu precipitation in HSLA steels is highly related with their mechanical properties and thus becomes an important hotspot industrially and scientifically. Cu is often artificially added in traditional HSLA steels such as shipbuilding steels to achieve precipitation strengthening [1–6]. In contrast, in some HSLA steels such as reactor pressure vessel steel, Cu often is considered as a solute impurity that induces destructive embrittlement when subjected to long-term neutron irradiation at ~ 400 °C [7–13]. Therefore, it is important to tailor the precipitation morphology of Cu-rich precipitates (CRPs) for attaining desired strength and toughness balance.

Actually, the characteristics of CRPs in aspect of size, number density, shape, etc., that determine final mechanical properties are largely dependent of the compositional and resultant structural evolution during heat treatment process, and the segregation of Ni and Mn at the precipitate/matrix interface significantly prohibits the growth of CRPs to large size [14–21]. In additional, the compositional evolution of CRPs provides important information for composition modification, processing optimization, and property improvement of Cu-containing steels. However,

Available online at http://link.springer.com/journal/40195.

✉ Jianfeng Gu
gujf@sjtu.edu.cn

[1] Institute of Materials Modification and Modelling, School of Materials Science and Engineering, Shanghai Jiao Tong University, Shanghai 200240, China

[2] Collaborative Innovation Center for Advanced Ship and Deep-Sea Exploration, Shanghai Jiao Tong University, Shanghai 200240, China

[3] Scholl of Nuclear Science and Engineering, Shanghai Jiao Tong University, Shanghai 200240, China

Published online: 16 October 2017

the size-dependent compositional evolution of CRPs has not been thoroughly clarified. In this paper, the CRPs formed in an isothermally aged HSLA steel were studied by atom probe tomography (APT), especially focusing on the compositional and morphological evolution of CRPs at their different precipitation stages.

2 Material and Experimental

The steel used was prepared by vacuum induction melting and cast into an 80 kg ingot. After homogenization and forging, the ingot was hot-rolled into the plate with a thickness reduction from 140 to 32 mm followed by air cooling. The steel plate was fully austenitized and solutionized at 900 °C for 30 min followed by quenching in water and then isothermally aged at 500 °C for 1, 4, 16, and 64 h. The nominal chemical composition of the steel is 0.04 C, 0.24 Si, 0.84 Mn, 1.15 Cu, 1.94 Ni, 0.51 Mo, 0.50 Cr, 0.043 Nb, 0.009 Ti, 0.03 Al, 0.004 N, 0.007 P, and 0.004 S (wt%).

The APT experiment, using an advanced Imago (now Cameca Instruments) local electrode atom probe (LEAP, 3000 HR, CAMECA, Gennevilliers, France) using voltage pulsing mode, was performed at a residual pressure of $\sim 3 \times 10^{-9}$ Pa and the specimen temperature of -223 °C, and with a pulse repetition frequency of 200 kHz, the pulse-voltage to dc-voltage ratio of 15%. The specimen for APT was prepared by using a standard two-stage electropolishing method [22]. Data analysis was performed by using the Imago Visualization and Analysis Software (IVAS). The Cu-rich precipitates (CRPs) are identified by 10 at.% Cu isoconcentration surfaces, and their sizes were represented by the diameter (D) of equivalent spherical volume of the surface.

3 Results and Discussion

Figure 1 shows APT reconstructed 3D distribution maps of the Cu-rich precipitates (CRPs) in the steel samples aged at 500 °C for different time. Generally, the CRPs increase in size and decrease in number density and evolve from initially spheroidal to more ellipsoidal or rodlike in morphology with prolonged aging time from 1 to 64 h. The nanoscale CRPs or Cu-rich clusters are almost uniformly distributed at their early nucleation stage, as shown in Fig. 1a. The formation of Cu nuclei can be promoted by Ni-rich clusters which are prevailingly formed during aging of Cu- and Ni-bearing steels [23]. The CRPs can directly nucleate in the Cu supersaturated ferritic matrix with the assisting of Ni-rich clusters and therefore exhibit a random distribution in the ferritic matrix. On the other hand, the nucleation and growth CRPs are more readily to correlate with the crystallographic defects such as dislocations and martensite lath boundaries LBs [24], which provide relative fast solute diffusion pathways of Cu atoms. The arrangements of CRPs in Fig. 1b probably outline these linear defects. Taking the scale of reconstructed maps into consideration, the CRPs in Fig. 1c are comparable in size to those in Fig. 1b. The CRPs undergo limited growth when the holding time prolonged form 4 to 16 h. One promising explanation is that Ni and Mn tend to segregate at the precipitate/matrix heterophase interfaces and therefore impede rapid growth of the CRPs [25–27]. Notably, some CRPs locate out of the atom map in Fig. 1c, because the reconstructed volume is relatively small. The presence of rodlike CRPs in Fig. 1d indicates the late growth stage of CRPs at aging for 64 h. However, not all CRPs are rodlike but most of them are larger in size than those formed for shorter aging time (Fig. 1a–c). This is probably attributed to the fact that the larger precipitates grow at expend of the smaller ones during the ripening process.

The size distribution of CRPs in the steel samples aged at 500 °C for different time is shown in Fig. 2, where the average size (precipitate diameter, D_p) and number densities (Nv) are also indicated. The size region of the CRPs with the highest frequency that represents the most prevailing CRPs gradually shifts from 2–3 to 4–5 nm with prolonged aging time from 1 to 64 h. Note, the CRPs will be underestimated in average size when some of the precipitates are partly located out of the APT reconstructed volume (see Fig. 1c). As a result, the frequency of smaller CRPs between 2 and 3 nm is exceptionally enhanced in Fig. 2c. The average size of CRPs increases from (2.37 ± 0.48) to (4.81 ± 1.46) nm with prolonged aging time. In addition, the standard deviation of the average size also gradually increases. It is possibly attributed to the presence of small CRPs that are either resulted from the coarsening of the precipitates or related to the limited APT reconstructed volume. The number density of the CRPs generally decreases from $(1.19 \pm 0.29) \times 10^{23}$ to $(1.95 \pm 0.35) \times 10^{22}$ m^{-3} with prolonged aging time. However, the precipitate density at 4 h aging $[(4.64 \pm 0.47) \times 10^{22}$ m$^{-3}]$ is relatively smaller than that at 16 h aging $[(5.32 \pm 0.76) \times 10^{22}$ m$^{-3}]$. The unordinary phenomena are possibly ascribed to the smaller APT data set in Fig. 1c. In addition, the preferential formation of CRPs at crystallographic defects often creates precipitate-free zones (PRZs) in the ferritic matrix [24]. When the PFZs are incorporated in the APT reconstructed volume, the number density of CRPs will be accordingly underestimated (Fig. 2b), and vice versa.

Figure 3 gives the proxigram concentration profiles of the selected CRPs marked by arrows in Fig. 1, where the morphology (shown by APT reconstructed map), size

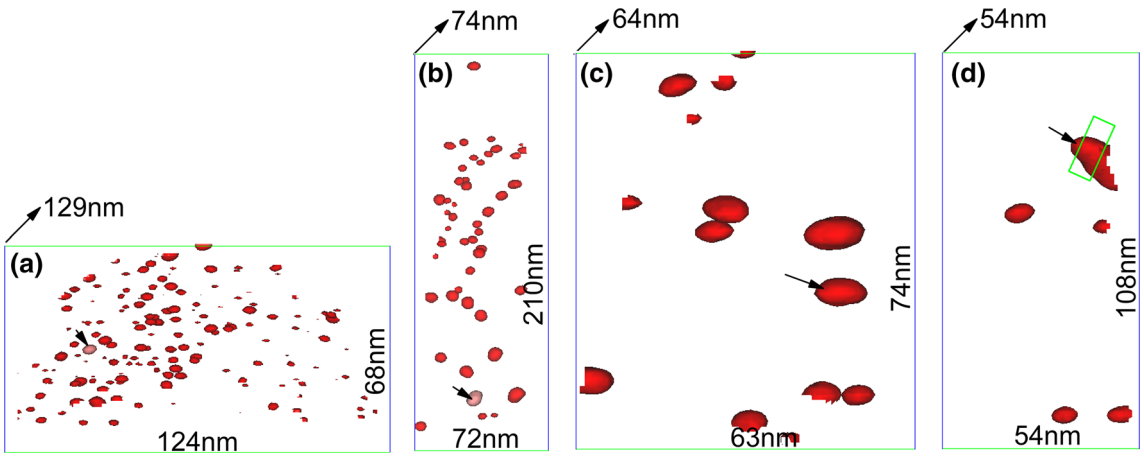

Fig. 1 APT reconstructed 3D distribution map of CRPs delineated by 10 at.% Cu isoconcentration surfaces in the steel samples isothermally aged at 500 °C for **a** 1 h, **b** 4 h, **c** 16 h, **d** 64 h. The CRPs marked by arrow are selected for further composition analysis

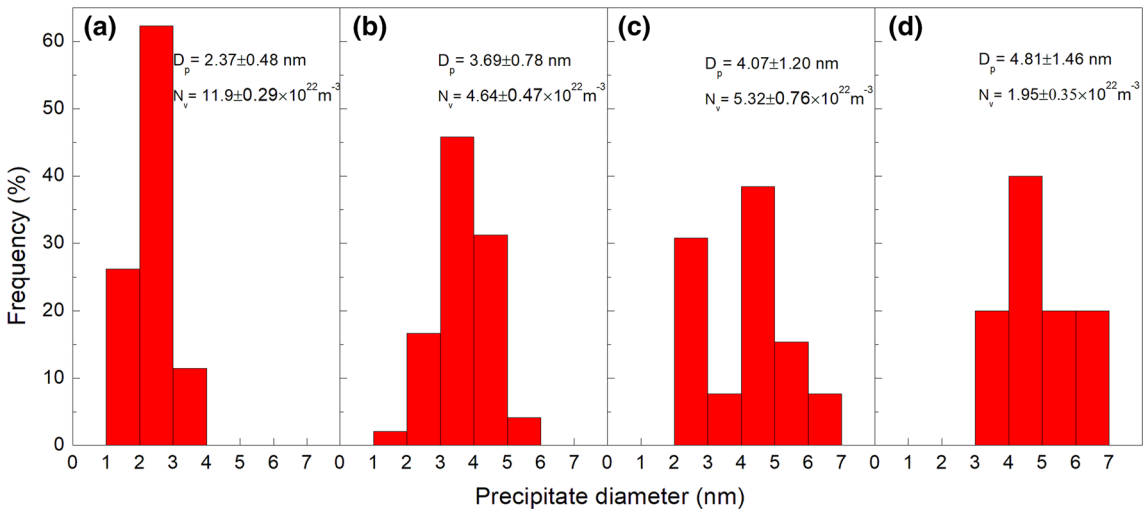

Fig. 2 Size distribution integrated with the average diameter (D_p), number density (N_v) of the CRPs in the steel samples quenched and aged at 500 °C for **a** 1 h, **b** 4 h, **c** 16 h,**d** 64 h

(represented by equivalent diameter, D), and compositions (within 10 at.% Cu isoconcentration surfaces) of the precipitates are also indicated. With prolonged aging time, the selected individual CRPs gradually increase from 6.6 to 13.2 nm in size and accordingly evolve from spheroidal to more ellipsoidal or rodlike in morphology. Meanwhile, the CRPs are rich in different amount of Fe, Ni and Mn. It seems that the CRP at aging for 1 h contains less Cu than that in the other aging conditions and thus is likely rich in more Fe, Ni and Mn. In light of the quantitative compositions, the CRPs contain less Fe and more Cu as well as slightly decreased Ni and gradually increased Mn in content. However, these solute atoms, especially Ni and Mn, are heterogeneously distributed from the matrix to the precipitate interiors, as indicated by the proxigram concentration profiles. When the CRP is relatively small (Fig. 3a), the precipitate interior contains ~ 75 at.% Cu and more than 20 at.% Fe as well as a comparatively high amount of Ni and Mn. Moreover, the deviations of the concentrations of individual solute atoms are relatively high due to the low total amount of atoms analyzed in every bin volume. When the CRPs increase in size with prolonged aging time (Figs. 3b–d), the precipitates contain as high as ~ 90 at.% Cu and nearly ~ 0 at.% Fe as well as decreased Ni and Mn, which are the compositions of typical CRPs in equilibrium state. Ni and Mn are likely prone to segregate at the precipitate/matrix heterophase interfaces. However, the intensity of segregation is different for the CRPs with different sizes. With increased size of the selected CRPs in an order of 7.6→9.2→13.2 nm, the peak concentrations of Ni and Mn at the precipitate/matrix interfaces increase roughly in the order of 5→6→8 at.% and 4→5→6 at.%, respectively. In addition, considering the initial nominal composition of the steel, Mn generally

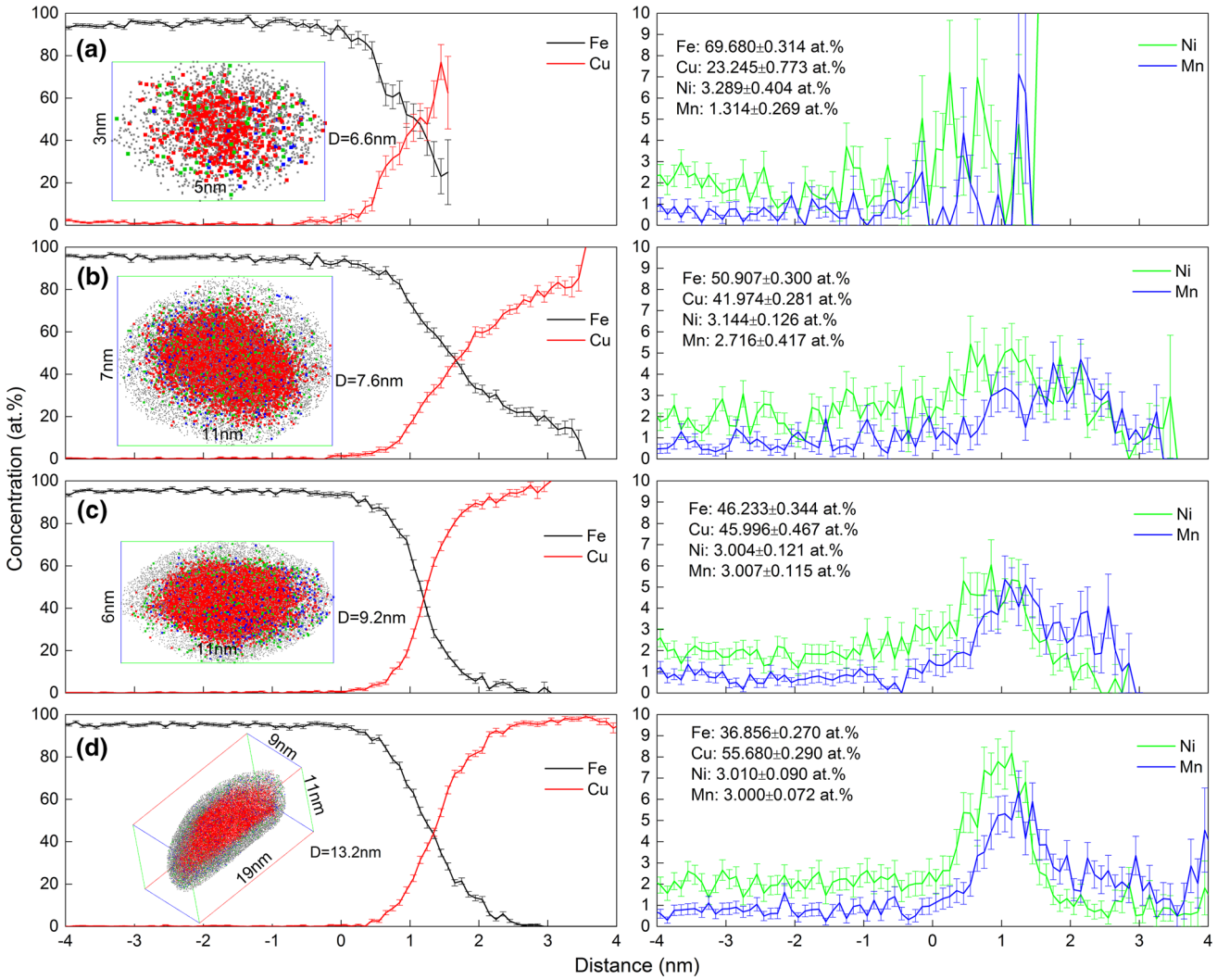

Fig. 3 Proxigram concentration profiles for Fe, Cu, Ni, and Mn with respect to 10 at.% Cu isoconcentration surfaces of the selected CRPs marked by arrow in Fig. 1, integrated with the APT reconstructed 3D atom maps, equivalent diameters, D_p, and composition of the separate CRPs. Steel samples aged at 500 °C for **a** 1 h, **b** 4 h, **c** 16 h, **d** 64 h

exhibits stronger tendency of enrichment than Ni in the precipitate interior, which suggests Mn is more readily to stay in the precipitate interior especially for the CRPs with more equilibrium compositions and hence larger size.

Figure 4 gives detail APT analysis of a representative coarsen CRP in the steel sample aged at 500 °C for 64 h, marked by green rectangle in Fig. 1d, showing (a) the 3D distribution of Cu, Ni, Mn, C, Mo, Cr, Fe, and Si and (b) the corresponding 1D composition profile along Z direction (blue line) in (a). Most of Cu precipitates out to contribute the formation of coarsened CRP, thereby leading to Cu depletion in the surround ferritic matrix. Only a limited few Fe and Ni are found in the CRP's interior, whereas Mn seemingly tends to retain within, as shown in Fig. 4b. Although both Ni and Mn are readily segregate at the precipitate/matrix boundary, Mn is prone to "stay" in the CRP's interior. Taking the nominal composition into account, it seems that the CRP contains comparable amount of Ni and higher amount of Mn compared with the initial content in solution. This means that Mn is more readily to enrich in the CRP's interior other than segregate at the precipitate/matrix interface. In addition, the fact the CRP depletes with the carbide-forming elements Mo, Cr, and C, as shown by atom distribution maps and composition profile, and makes the co-precipitation of CRPs with alloyed carbide thermodynamically possible. Moreover, the CRP is free of Si that tends to diffuse toward the ferritic matrix during CRPs' growth [17].

Figure 5 displays schematic illustration of compositional evolution of the CRPs. At the early nucleation stage, Cu atoms diffuse to replace Fe atoms in the crystal lattice of ferritic matrix and further to form the nanoscale Cu-rich clusters. At the initial nucleation stage, Fe, Cu, Ni, and Mn are generally randomly distributed, as shown in Fig. 4a.

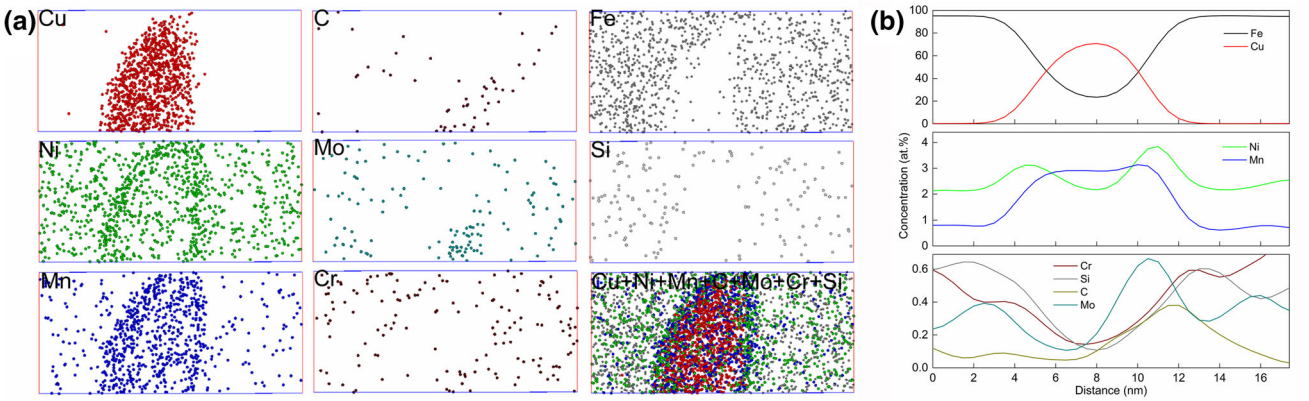

Fig. 4 **a** APT reconstructed 3D atom distribution map of Cu, Ni, Mn, C, Cr, Mo, Si, and Fe atoms in and around a selected CRP with elongated rod-shaped marked green rectangle in Fig. 1d. **b** Composition profile of the CRP along Z direction (blue line) in **a**, showing the redistribution behavior of the solute atoms across the precipitate. Sample tempered at 500 °C for 64 h

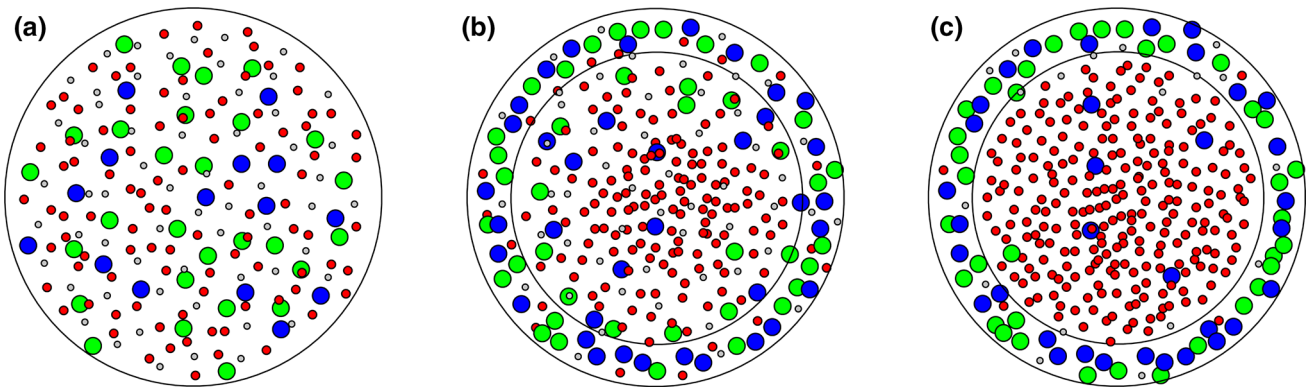

Fig. 5 Schematic illustration of compositional evolution of CRPs showing the distribution of Cu (red), Fe (gray), Ni (green), and Mn (blue) in the CRPs approaching their equilibrium composition

The crystallographic defects and the preexisting Ni-rich cluster would promote the Cu clustering. The Cu-rich clusters are considered to be BCC-structured and coherent with the surrounding ferritic matrix [28–30]. During the growth of the Cu-rich clusters, Fe is continuously depleted into ferritic matrix and, Ni and Mn gradually diffuse to the precipitate/matrix heterophase interface, contributing to the development of a composition induced core–shell structure. At the same time, the structure of the CRPs evolves from BCC to transitional structures of 9R and 3R. The compositional and structural evolution is thought to largely reduce the strain energy and interfacial energy [31, 32]. With the growth process proceeding, the CRPs eventually reach their equilibrium composition with only a little Fe and Ni but some Mn in the precipitate interior. Ni and most of Mn segregate at the precipitate/matrix interface to inhibit fast coarsening of the CRPs, and Fe is almost expelled into the matrix. Meanwhile, a FCC structure is formed along with the development of an ellipsoidal or rodlike morphology [17].

4 Conclusion

The Cu precipitation in a high-strength low-alloy steel isothermally aged at 500 °C for different time is characterized by using atom probe tomography. With prolonged aging time at 500 °C, the CRPs generally increase in size and decrease in number density, and gradually evolve from spherical to more ellipsoidal in morphology. The small CRPs are rich in a relatively high amount of Fe and a certain amount of Ni and Mn, and these atoms exhibit relatively high composition deviation. The large CRPs contain more Cu and less Fe. Ni and Mn are readily to segregate at the Cu-rich precipitate/matrix interface. The concentration of Mn is higher than that of Ni in the precipitate interior especially when the precipitate is large in size. Compared to Ni, Mn is more readily to enrich in the CRP's interior other than segregate at the precipitate/matrix interface. In addition, the formation of CRPs is in association with alloyed carbide.

Acknowledgements One of the authors, Qingdong Liu, thanks to Mrs Qifeng Zeng at Shanghai Nuclear Engineering and Research & Design Institute, China, for her great support to this research.

References

[1] E.J. Czyryca, R.E. Link, R.J. Wong, D.A. Aylor, T.W. Montemarano, J.P. Gudas, Nav. Eng. J. **102**, 63 (1990)
[2] S. Thompson, G. Krauss, Metall. Mater. Trans. A **27**, 1573 (1996)
[3] S. Vaynman, D. Isheim, R.P. Kolli, S.P. Bhat, D.N. Seidman, M.E. Fine, Metall. Mater. Trans. A **39**, 363 (2008)
[4] R.D.K. Misra, Z. Jia, R. O′Malley, S.J. Jansto. Mater. Sci. Eng. A **528**, 8772 (2011)
[5] Z. Zhang, C. Liu, Y. Wen, A. Hirata, S. Guo, G. Chen, M. Chen, B. Chin, Metall. Mater. Trans. A **43**, 351 (2012)
[6] R.P. Kolli, D.N. Seidman, in *Heat Treatment of Copper Precipitation-Strengthened Steels, ASM Handbook, Volume 4D, Heat Treating of Irons and Steels*, ed by J. Dossett, G.E. Totten (ASM International, Materials Park 2014), pp. 188
[7] G.E. Lucas, J. Nucl. Mater. **407**, 59 (2010)
[8] Reports: Integrity of Reactor Pressure Vessels in Nuclear Power Plants: Assessment of Irradiation Embrittlement Effects in Reactor Pressure Vessel Steels, IAEA Nuclear Energy Series. No. NP-T-3.11. International Atomic Agency, Vienna, 2009
[9] G.R. Odette, B.D. Wirth, D.J. Bacon, N.M. Ghoniem, MRS Bull. **26**, 176 (2001)
[10] T. Takeuchi, A. Kuramoto, J. Kameda, T. Toyama, Y. Nagai, M. Hasegawa, T. Ohkubo, T. Yoshiie, Y. Nishiyama, K. Onizawa, J. Nucl. Mater. **402**, 93 (2010)
[11] M.K. Miller, K.F. Russell, J. Nucl. Mater. **372**, 145 (2007)
[12] G. Xu, L.L. Cai, L. Feng, B.X. Zhou, J.A. Wang, H.S. Zhang, Acta Metall. Sin. **48**, 753 (2012). **(in Chinese)**
[13] Z. Lu, Acta Metall. Sin. **47**, 777 (2011). **(in Chinese)**
[14] D. Isheim, R.P. Kolli, M.E. Fine, D.N. Seidman, Scr. Mater. **55**, 35 (2006)
[15] R.P. Kolli, D.N. Seidman, Microsc. Microanal. **13**, 272 (2007)
[16] R.P. Kolli, Z. Mao, D.T. Keane, D.N. Seidman, Appl. Phys. Lett. **91**, 241903 (2007)
[17] R.P. Kolli, D.N. Seidman, Acta Mater. **56**, 2073 (2008)
[18] M.D. Mulholland, D.N. Seidman, Scr. Mater. **60**, 992 (2009)
[19] M.D. Mulholland, D.N. Seidman, Acta Mater. **59**, 1881 (2011)
[20] Z.W. Zhang, C.T. Liu, M.K. Miller, X. Wang, Y.R. Wen, T. Fujita, A. Hirata, M.W. Chen, G. Chen, B.A. Chin, Sci. Rep. **3**, 1327 (2013)
[21] R.P. Kolli, D.N. Seidman, Microsc. Microanal. **20**, 1727 (2014)
[22] M.K. Miller, *Atom Probe Tomography: Analysis at the Atomic Level* (Kluwer Academic/Plenum Publishers, New York, 2000), p. 26
[23] Q.D. Liu, J.F. Gu, W.Q. Liu. Metall. Mater. Trans. A **44**, 4434 (2013)
[24] Q.D. Liu, S.J. Zhao, MRS Commun. **4**, 127 (2012)
[25] B.L. Tiemens, A.K. Sachdev, R.K. Mishra, G.B. Olson, Metall. Mater. Trans. A **43**, 3626 (2012)
[26] Q.D. Liu, W.Q. Liu, X.Y. Xiong, J. Mater. Res. **27**, 1060 (2012)
[27] Q.D. Liu, S.J. Zhao, Metall. Mater. Trans. A **44**, 163 (2013)
[28] R. Monzen, M. Iguchi, M.L. Jenkins, Philos. Mag. Lett. **80**, 137 (2000)
[29] P.J. Othen, M.L. Jenkins, G.D.W. Smith, Philos. Mag. A **70**, 1 (1994)
[30] R. Monzen, M.L. Jenkins, A.P. Sutton, Philos. Mag. **80**, 711 (2000)
[31] G. Xu, D.F. Chu, L.L. Cai, B.X. Zhou, W. Wang, J.C. Peng, Acta Metall. Sin. **47**, 905 (2011). **(in Chinese)**
[32] R. Monzen, K. Takada, C. Watanabe, ISIJ Int. **44**, 442 (2004)